Mesoporous Films

DOI: 10.1002/anie.201008192

A Mesoporous γ-Alumina Film with Vertical Mesoporosity: The Unusual Conversion from a *Im*$\bar{3}$*m* Mesostructure to Vertically Oriented γ-Alumina Nanowires

*Hamid Oveisi, Xiangfen Jiang, Masataka Imura, Yoshihiro Nemoto, Yasuhiro Sakamoto, and Yusuke Yamauchi**

Since their discovery,[1,2] mesoporous materials of various compositions generated by self-organization of surfactants have attracted considerable interest as one of the key materials in current nanotechnology. Ordered mesoporous materials with various morphologies, such as nanoparticles, monoliths, spheres, rods, fibers, and films, have been prepared so far. Among them, mesoporous films with regularly arranged mesospace have attracted broad interest because of their wide applicability in optics, electronics, sensing, and catalysis.[3–7] Macroscopic alignment of the mesopore space and its control in films are especially significant for advanced nanomaterials with controlled functions.[8–11] In general, the mesopore spaces in the films are oriented parallel to the substrates. This fact seriously devalues the advantages of mesoporous films because the lying mesospace suppresses effective diffusion of guest species from the outside.[12] If vertical porosity can be engineered, great potential applications can be expected in the fields of chemical sensors and separations.[12]

Worldwide, research on perpendicular mesoporosity is highly competitive. Partial perpendicular alignment of one-dimensional (1D) mesochannels has been achieved by the use of modified surfaces,[13,14] or magnetic[15,16] and electric fields.[17] The ternary surfactant system[18] or the microwave irradiation method[19] have led to the creation of a completely perpendicular orientation, but the system is presently limited to the formation of powdery samples. Perpendicularly arranged mesochannels have been generated inside the straight pores of anodic porous alumina,[20,21] but continuous mesoporous films can not be obtained. Continuous films with perpendicular mesochannels have been successfully prepared by utilizing unique microphase separations of self-assembling molecules, such as block copolymers.[22,23] However, the thermal and mechanical stability is low due to pore walls consisting of flexible compositions, such as organosilica and polymers.

Herein, we prepare a continuous mesoporous film consisting of γ-alumina nanowires with perfect vertical mesoporosity by utilizing the unusual mesostructural conversion from the cage-type *Im*$\bar{3}$*m* mesostructure during the crystallization of alumina frameworks. Recently, Wu and Kuroda et al. proposed an elegant formation of mesoporous anatase (TiO_2) films with vertical mesoporosity by a structural transformation from $P6_3/mmc$ (i.e., ABABAB stacking of mesopores).[24] Unfortunately, however, another close packing mesostructure, *Fm*$\bar{3}$*m* (i.e., ABCABC stacking of mesopores), was mixed in the original TiO_2 films before the crystallization.[24] Therefore, the resulting mesospace did not pass through the entire film thickness, as confirmed by SEM.[24] Because both $P6_3/mmc$ and *Fm*$\bar{3}$*m* are very stable close-packing mesostructures, it is generally difficult to selectively form the single phase.

To solve the inevitable problem, here, we propose an alternative interesting conversion from a cage-type *Im*$\bar{3}$*m* mesostructure. In our system, by using an optimized precursor solution consisting of an F127 surfactant and aluminum alkoxide, mesoporous Al_2O_3 with only an *Im*$\bar{3}$*m* mesostructure can be prepared. After the crystallization, all the γ-alumina nanowires can grow continuously from the substrate to the film surface, achieving complete vertical mesoporosity. Furthermore, the obtained γ-alumina film has much higher thermal stability than the TiO_2 system[24] due to crystallization at over 1000 °C. A wide range of applications, such as adsorption, separation, catalysis, and catalyst support can be expected.

The mesoporous γ-alumina film was prepared by spin-coating the precursor solution on silicon substrates. The precursor solution was prepared by mixing a triblock copolymer Pluronic F127 ($EO_{106}PO_{70}EO_{106}$), aluminum tri-*n*-butoxide, hydrochloric acid, and ethanol under stirring. After the coating, the as-prepared thin films were aged at

[*] X. Jiang,[+] Dr. M. Imura, Dr. Y. Nemoto, Prof. Dr. Y. Yamauchi
World Premier International (WPI) Research Center for Materials Nanoarchitectonics (MANA)
National Institute for Materials Science (NIMS)
1-1 Namiki, Tsukuba, Ibaraki 305-0044 (Japan)
E-mail: Yamauchi.Yusuke@nims.go.jp
X. Jiang,[+] Prof. Dr. Y. Yamauchi
Faculty of Science and Engineering, Waseda University
3-4-1 Okubo, Shinjuku, Tokyo 169-8555 (Japan)
Prof. Dr. Y. Sakamoto
Nanoscience and Nanotechnology Research Center
Osaka Prefecture University, Sakai 599-8570 (Japan)
Prof. Dr. Y. Yamauchi
Precursory Research for Embryonic Science and Technology (PRESTO)
Japan Science and Technology Agency (JST)
4-1-8 Honcho, Kawaguchi, Saitama 332-0012 (Japan)
Dr. H. Oveisi[+]
Metallurgy and Materials Engineering Department
Tarbiat Moallem University of Sabzevar, Sabzevar 397, Iran
[+] These authors equally contributed this work.

Supporting information for this article is available on the WWW under http://dx.doi.org/10.1002/anie.201008192.

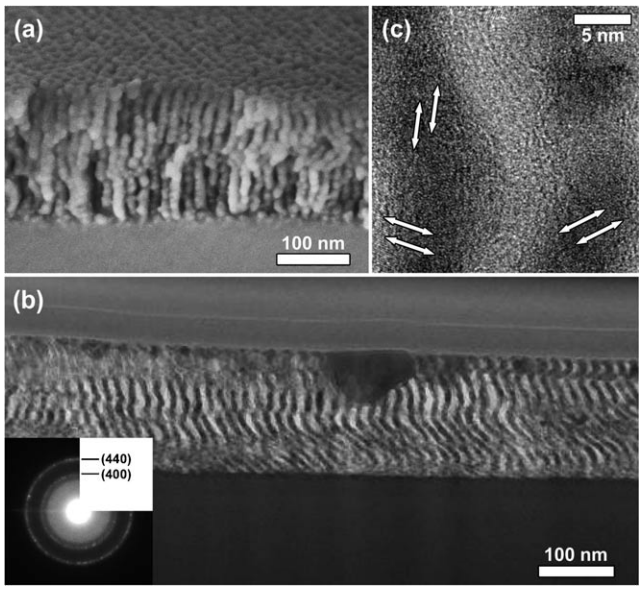

Figure 1. Cross-sectional a) SEM and b, c) TEM images of the mesoporous γ-alumina film after calcination at 1000 °C. The inset image shows selected-area ED patterns taken from a 100 nm^2 area. The lattice fringes are indicated by the arrows in c).

−20 °C with 20 % relative humidity for 2 h. After the aging, the films were calcined in an air atmosphere at 1000 °C. Details are given in the Experimental Section.

Figure 1 shows cross-sectional SEM and TEM images of the films after calcinations at 1000 °C. Surprisingly, vertically oriented nanowires were clearly observable over the entire film. They were periodically distributed and partially interconnected with each other. From the substrate to the top surface, each nanowire grew continuously, creating perfect vertical mesoporosity among the nanowires. On the top surface, two different kinds of arrangements of nanowires were confirmed. In most regions (> 90 %), a fourfold symmetry was observed (Figure 2 a-3; Supporting Information, Figure S1a-2), while, in a few others, a sixfold symmetry existed (Figure 2 b-3; Supporting Information, Figure S1b-2). The selected area electron diffraction (ED) showed ringlike patterns assignable to the (400) and (440) planes of the γ-alumina phase (Figure 1 b, inset). The HR-TEM image indicated that the alumina wires consisted of very small γ-alumina nanocrystals less than 5 nm in diameter (Figure 1 c). The lattice fringes were randomly oriented without crystal growth in a specific direction. Wide-angle XRD patterns also indicated the formation of the γ-alumina crystals (Supporting Information, Figure S2).

To understand the formation mechanism, the mesoporous alumina film before the crystallization (i.e., calcined at 400 °C) was carefully investigated. Typical TEM images derived from an $Im\bar{3}m$ mesostructure were observable in the powdery samples scratched from the substrate (Figure S3). The cross-sectional TEM image of the film can be regarded as viewed from the ⟨100⟩ and ⟨110⟩ zone axes of the $Im\bar{3}m$ mesostructure with the ⟨001⟩-direction oriented perpendicular to the substrate (Figure S4). The observed $Im\bar{3}m$ mesostructure largely shrank along the c axis (a, $b = 19$ nm, $c = 7$ nm). The only vertical distance (c) in the unit cell

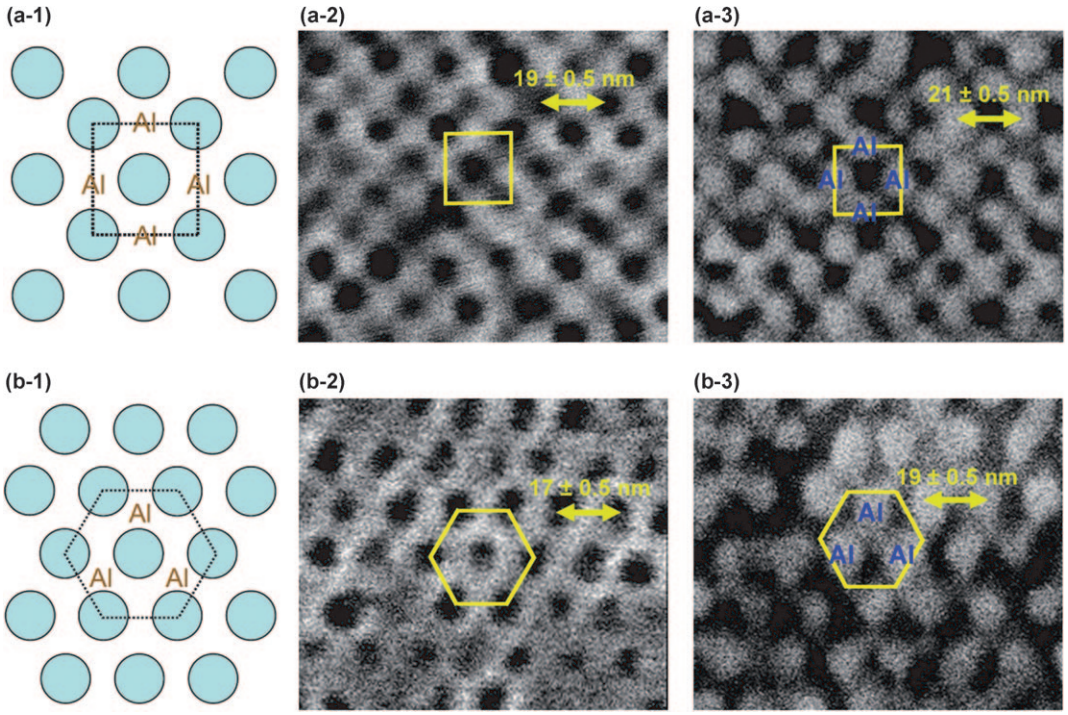

Figure 2. Understanding of the mesostructural conversion process from $Im\bar{3}m$ to vertically oriented nanowires. (a-1, b-1): Top views of mesoporous films with two different $Im\bar{3}m$ orientations. The ⟨001⟩ direction (a-1) and the ⟨111⟩ direction (b-1) of the $Im\bar{3}m$ are oriented perpendicular to the substrate. (a-2, b-2): Top surface SEM images of the mesoporous alumina film calcined at 400 °C (before the mesostructural conversion). (a-3, b-3): Top surface SEM images of the mesoporous alumina film calcined at 1000 °C (after the mesostructural conversion).

showed a 63% reduction ($c \rightarrow c'$), which was in good agreement with the degree of shrinkage in the film thickness (60%). Through the calcination at 400°C, the original film thickness decreased by around 60% (Figure S5). Taking this large shrinkage along the c axis into account, we theoretically calculated how the relationship between the horizontal distance and the vertical distance in one unit cell changes on calcination (Figure S6). Both ⟨100⟩ and ⟨110⟩ views before and after the shrinkage were examined in Figure S6. The calculated values were almost the same as the values (c'/a ratios) observed in Figure S4.

SEM observation on the top surface confirmed that the uniform mesopores were periodically arranged. A fourfold arrangement was observed over the entire area in almost all parts of the films (Figure 2a-2; Supporting Information, Figures S1a-1 and S7). The fourfold arrangement can be viewed along the ⟨001⟩ zone axis. This can be understood from the simulated model of the top views of oriented $Im\bar{3}m$ (Figure S8). In a very small region, a sixfold arrangement of the mesopores was also observed on the film surface (Figure 2b-2; Supporting Information, Figures S1b-1 and S7), indicating that the ⟨111⟩ zone axis of $Im\bar{3}m$ was partially oriented perpendicularly to the substrate.

There are three possible orientations of the $Im\bar{3}m$ mesostructure in the films (Figure S8), in which the ⟨001⟩ direction, the ⟨111⟩ direction, or the ⟨110⟩ direction of the mesostructure is oriented perpendicularly to the substrate. Previously, Alberious et al. prepared mesoporous titania thin films with an $Im\bar{3}m$ mesostructure by using titanium tetraethoxide ($Ti(OC_2H_5)_4$) as a titanium source and the triblock copolymer P123 as a surfactant.[25] In their case, the ⟨001⟩ direction was oriented perpendicularly to the substrate. On the other hand, Grosso et al. used $TiCl_4$ as a titanium source and F127 as the surfactant to generate mesoporous titania thin films in which the ⟨110⟩ direction of the $Im\bar{3}m$ mesostructure was perpendicular to the substrate.[26] In addition, recently, it was reported that the ⟨111⟩ direction of the $Im\bar{3}m$ mesostructure was oriented perpendicularly to the substrate.[27] These examples indicate that a slight difference in the inorganic sources, surfactants, and synthetic processes affects not only the final mesostructure but also its orientation.

In the present case, the TEM and SEM images strongly indicated that the $Im\bar{3}m$ mesostructure with the ⟨001⟩-direction oriented perpendicular to the substrates was a main component in the film. However, another possibility, namely the formation of the cage-type $Fm\bar{3}m$ mesostructure should also be considered here. This is because, when the ⟨001⟩ direction of the $Fm\bar{3}m$ mesostructure is vertically oriented to the substrate (Figure S9), the fourfold arrangement is simulated as the top-surface image (similar to that shown in Figure 2a-2). The models of both the ⟨100⟩ and ⟨110⟩ views of the $Fm\bar{3}m$ mesostructure with the ⟨001⟩ direction oriented perpendicular to the substrate were examined (Supporting Information, Figure S10). The unit cell of the ⟨100⟩-viewed $Fm\bar{3}m$ mesostructure resembles the ⟨110⟩ view of the $Im\bar{3}m$ mesostructure with the ⟨001⟩ direction oriented perpendicular to the substrate (Figure S6). Also, the half of unit cell of the ⟨110⟩-viewed $Fm\bar{3}m$ mesostructure resembles the ⟨100⟩ view of the $Im\bar{3}m$ mesostructure with the ⟨001⟩-direction oriented perpendicular to the substrate (Figure S6). The relative ratios of the vertical distance to the horizontal distance were calculated after 60% reduction in the film thicknesses (Figure S10). The simulated values, however, were quite different from those of the $Im\bar{3}m$ system (Figure S6), which was so far from the obtained c'/a values in Figure S4. Therefore, we can rule out the possibility of the formation of the $Fm\bar{3}m$ mesostructure.

The present mesostructural transformation from the $Im\bar{3}m$ alumina film is created by the large contraction of the film (in total, around 80%) along the perpendicular direction to the substrate, which is induced by the crystallization of the frameworks (Figure S5). Two different orientations of an $Im\bar{3}m$ mesostructure existing in the film before the crystallization are illustrated in Figure S11. These projection images are viewed along the perpendicular direction to the substrate. The white area in these images denotes the region of alumina existing throughout the film thickness. Upon the calcination, this amorphous alumina framework shrinks along the perpendicular direction to the substrate. The crystal growth is then generally thought to occur in the inner parts of the frameworks. Therefore, at the initial stage of the crystallization, the seeds (very small nuclei) are supposed to be generated in the central parts of the red-colored "Al" region in Figure 2a-1, 2b-1, and Figure S11 in the Supporting Information. Thereafter, the crystal growth proceeds by diffusing amorphous alumina to the nuclei. At the early stage of the crystallization, γ-alumina crystals surrounded by an amorphous phase cannot reach the mesopore spaces. The manner in which the perpendicular mesospace is formed can be understood from the cross-sectional view (Figure S12). As the calcination temperatures increased (i.e., the increase in the degree of crystallization of the alumina), the neighboring mesopores were connected and merged along the perpendicular direction due to the large shrinkage (see Figure S5c). At calcination temperatures below 900°C, the spherical mesopores still remained due to insufficient crystallization in the framework (Figure S12b). However, by applying calcination temperatures over 1000°C, the crystallization was almost completes, leading to vertical mesospaces (Figure 1). The intervals of the mesopores before the calcination are almost identical to those of the alumina nanowires after the calcination (Figure 2). This evidence also supports the mechanism suggested above. The obtained vertical mesoporosity was retained up to 1100°C. With further increase of the calcination temperature, crystal growth of γ-alumina in the frameworks proceeded to destroy the ordered arrangements of the nanowires (Figure S13).

In conclusion, we successfully synthesized a crack-free mesoporous γ-alumina film with vertical mesoporosity by the unusual conversion from a cage-type $Im\bar{3}m$ mesostructure. Each nanowire was well crystallized to give a γ-alumina phase by a calcination process at 1000°C. The vertical mesoporosity is created by uniform voids among the nanowires, which will be important for potential applications, such as highly sensitive sensors and highly reactive catalyst supports.

Generally, porous alumina materials can used in a wide range of applications, such as adsorption, separation, catalysis,

and catalyst support. Several types of mesoporous alumina have been recently reported by using hard- and soft-templating methods.[28–30] However, the mesoporous alumina materials have been mainly prepared in power form. For practical applications as molecular membranes and separators, a continuous film is a more suitable morphology. Furthermore, the pore architecture in alumina films plays a major role in their performance. In previous work, Grosso and Sanchez et al. have successfully prepared an ordered mesoporous alumina film with cage-type mesostructure by using KLE surfactants, but 1D mesoporosity passing through the entire film thicknesses was not formed.[31] Vertical mesoporosity in the films can drastically accelerate diffusion of the guest molecules from the outside, which is an ideal pore architecture for the applications.[12] Here, we achieved the synthesis of mesoporous γ-alumina films combining ideal vertical mesospace and crystalline frameworks with good thermal stability. This is the first report on mesoporous γ-alumina films with vertical mesoporosity. It should be possible to extend this work to provide a general synthetic methodology for other metal oxides in the future.

Experimental Section

Materials: Triblock copolymer pluronic F127 ($EO_{106}PO_{70}EO_{106}$) with a molar weight of 12600 g mol^{-1} was purchased from Aldrich and used as the structure-directing agent for the fabrication of the mesoporous alumina films in this study. Concentrated hydrochloric acid (37 wt %), ethanol, and aluminum tri-*n*-butoxide were obtained from Wako Co. and used as a catalyst, solvent, and aluminum source, respectively.

Synthesis of ordered mesoporous alumina films: The precursor solution was prepared according to the following procedure. Aluminum tri-*n*-butoxide (2.46 g) was added to a solution of 37 wt % hydrochloric acid (1.71 g) and absolute ethanol (4.74 g) under stirring. After 15 min of vigorous stirring, a solution of Pluronic F127 (1.00 g) dissolved in absolute ethanol (9.48 g) was added to this solution. Then, after stirring for another 6 h at 40 °C, the clear precursor solution was spin-coated on clean silicon substrates at 23 °C and 50 % relative humidity. The spinning speed and time were fixed at 3000 rpm and 30 s, respectively. The as-prepared thin films were then aged at −20 °C with 20 % relative humidity for 2 h. After the aging, the films were calcined in air at 1000 °C for 4 h with a ramp rate of 1 °C min^{-1}.

Characterization: The surface morphology of the thin film was observed with a field-emission scanning electron microscope. Field-emission scanning electron microscope (Hitachi S-4800 SEM) images were taken by using 5 kV acceleration voltages without coating to avoid covering of the pores by coating. The highly ordered mesoporous texture was confirmed by a JEOL-JEM 2100F TEM. The accelerating voltage of the electron beam was 200 kV.

Received: December 26, 2010
Published online: June 17, 2011

Keywords: alumina · $Im\bar{3}m$ mesostructure · mesoporous films · mesoporous materials · vertical mesoporosity

[1] a) T. Yanagisawa, T. Shimizu, K. Kuroda, C. Kato, *Bull. Chem. Soc. Jpn.* **1990**, *63*, 988; b) T. Yanagisawa, T. Shimizu, K. Kuroda, C. Kato, *Bull. Chem. Soc. Jpn.* **1990**, *63*, 1535.
[2] C. T. Kresge, M. E. Leonowicz, W. J. Roth, J. C. Vartuli, J. S. Beck, *Nature* **1992**, *359*, 710.
[3] a) M. Ogawa, *J. Am. Chem. Soc.* **1994**, *116*, 7941; b) M. Ogawa, *Chem. Commun.* **1996**, 1149.
[4] I. A. Aksay, M. Trau, S. Manne, I. Honma, N. Yao, L. Zhou, P. Fenter, P. M. Eisenberger, S. M. Gruner, *Science* **1996**, *273*, 892.
[5] H. Yang, A. Kuperman, N. Coombs, S. Mamiche-Afara, G. A. Ozin, *Nature* **1996**, *379*, 703.
[6] Y. F. Lu, R. Ganguli, C. A. Drewien, M. T. Anderson, C. J. Brinker, W. L. Gong, Y. X. Guo, H. Soyez, B. Dunn, M. H. Huang, J. I. Zink, *Nature* **1997**, *389*, 364.
[7] S. H. Tolbert, T. E. Schäffer, J. Feng, P. K. Hansma, G. D. Stucky, *Chem. Mater.* **1997**, *9*, 1962.
[8] H. Miyata, T. Suzuki, A. Fukuoka, T. Sawada, M. Watanabe, T. Noma, K. Takada, T. Mukaide, K. Kuroda, *Nat. Mater.* **2004**, *3*, 651.
[9] A. Fukuoka, H. Miyata, K. Kuroda, *Chem. Commun.* **2003**, 284.
[10] W. C. Molenkamp, M. Watanabe, H. Miyata, S. H. Tolbert, *J. Am. Chem. Soc.* **2004**, *126*, 4476.
[11] I. B. Martini, I. M. Craig, W. C. Molenkamp, H. Miyata, S. H. Tolbert, B. J. Schwartz, *Nat. Nanotechnol.* **2007**, *2*, 647.
[12] H. K. M. Tanaka, Y. Yamauchi, T. Kurihara, Y. Sakka, K. Kuroda, A. P. Mills, Jr., *Adv. Mater.* **2008**, *20*, 4728.
[13] a) V. R. Koganti, S. E. Rankin, *J. Phys. Chem. B* **2005**, *109*, 3279; b) V. R. Koganti, D. Dunphy, V. Gowrishankar, M. D. McGehee, X. F. Li, J. Wang, S. E. Rankin, *Nano Lett.* **2006**, *6*, 2567.
[14] a) Y. Yamauchi, T. Nagaura, S. Inoue, *Chem. Asian J.* **2009**, *4*, 1059; b) Y. Yamauchi, T. Nagaura, A. Ishikawa, T. Chikyow, S. Inoue, *J. Am. Chem. Soc.* **2008**, *130*, 10165.
[15] Y. Yamauchi, M. Sawada, M. Komatsu, A. Sugiyama, T. Osaka, N. Hirota, Y. Sakka, K. Kuroda, *Chem. Asian J.* **2007**, *2*, 1505.
[16] S. H. Tolbert, A. Firouzi, G. D. Stucky, B. F. Chmelka, *Science* **1997**, *278*, 264.
[17] K. Kuraoka, Y. Tanaka, M. Yamashita, T. Yazawa, *Chem. Commun.* **2004**, 1198.
[18] B. C. Chen, H. P. Lin, M. C. Chao, C. Y. Mou, C. Y. Tang, *Adv. Mater.* **2004**, *16*, 1657.
[19] Sujandi, S. E. Park, D. S. Han, S. C. Han, M. J. Jin, T. Ohsuna, *Chem. Commun.* **2006**, 4131.
[20] A. Yamaguchi, F. Uejo, T. Yoda, T. Uchida, Y. Tanamura, T. Yamashita, N. Teramae, *Nat. Mater.* **2004**, *3*, 337.
[21] Q. Lu, F. Gao, S. Komarneni, T. E. Mallouk, *J. Am. Chem. Soc.* **2004**, *126*, 8650.
[22] E. M. Freer, L. E. Krupp, W. D. Hinsberg, P. M. Rice, J. L. Hedrick, J. N. Cha, R. D. Miller, H. C. Kim, *Nano Lett.* **2005**, *5*, 2014.
[23] T. Thurn-Albrecht, R. Steiner, J. DeRouchey, C. M. Stafford, E. Huang, M. Bal, M. Tuominen, C. J. Hawker, T. Russell, *Adv. Mater.* **2000**, *12*, 787.
[24] C. W. Wu, T. Ohsuna, M. Kuwabara, K. Kuroda, *J. Am. Chem. Soc.* **2006**, *128*, 4544.
[25] P. C. A. Alberius, K. L. Frindell, R. C. Hayward, E. J. Karmer, G. D. Stucky, B. F. Chmelka, *Chem. Mater.* **2002**, *14*, 3284.
[26] D. Grosso, G. J. A. A. Soller-Illia, E. L. Crepaldi, F. Cangol, C. Sinturel, A. Bourgeois, A. B. Bruneau, H. Amenitsch, P. A. Albouy, C. Sanchez, *Chem. Mater.* **2003**, *15*, 4562.
[27] C. W. Koh, U. H. Lee, J. K. Song, H. R. Lee, M. H. Kim, M. Suh, Y. U. Kwon, *Chem. Asian J.* **2008**, *3*, 862.
[28] Z. Wu, Q. Li, D. Feng, P. A. Webley, D. Zhao, *J. Am. Chem. Soc.* **2010**, *132*, 12042.
[29] J. P. Dacquin, J. P. Dacquin, J. Dhainaut, D. Duprez, S. Royer, A. F. Lee, K. Wilson, *J. Am. Chem. Soc.* **2009**, *131*, 12896.
[30] C. Boissière, L. Nicole, C. Gervais, F. Babonneau, M. Antonietti, H. Amenitsch, C. Sanchez, D. Grosso, *Chem. Mater.* **2006**, *18*, 5238–5243.
[31] M. Kuemmel, D. Grosso, C. Boissière, B. Smarsly, T. Brezesinski, P. A. Albouy, H. Amenitsch, C. Sanchez, *Angew. Chem.* **2005**, *117*, 4665–4668; *Angew. Chem. Int. Ed.* **2005**, *44*, 4589–4592.

